Simulations of fast neutrino flavor conversions with interactions in inhomogeneous media

Günter Sigl*

Universität Hamburg, II. Institute for Theoretical Physics, Luruper Chaussee 149, 22761 Hamburg, Germany

(Received 6 October 2021; accepted 18 January 2022; published 10 February 2022)

We investigate toy models for spatial and temporal instabilities in collective neutrino oscillations induced by neutrino self-interactions, with special emphasis on inhomogeneous systems with densities following a profile. Simulations are based on a *Mathematica* program that solves the Liouville equation with or without vacuum terms, refractive terms from a background medium, and neutrino-neutrino forward scattering, in one space dimension and in time. A discrete number of momentum modes are characterized by the neutrino velocity projection on the spatial direction. We also consider the effects of charged current interaction source terms and neutral current scattering contributions. We find that refractive effects from the medium, in particular for density distributions with a profile, and neutral current nonforward scattering off the background medium can strongly influence fast collective flavor transformations. Specifically we find that if both are present, fast flavor conversions can be strongly suppressed or at least delayed.

DOI: 10.1103/PhysRevD.105.043005

I. INTRODUCTION

In environments with high neutrino densities the self-coupling of the known active electron-, muon-, and tau-neutrinos leads to interesting but at the same time complicated nonlinear effects. For mass splittings Δm^2 of neutrinos of momentum p the interplay between vacuum oscillations with frequency $\omega = \Delta m^2/(2p)$ and self-coupling corresponding to a rate $\mu \sim \sqrt{2} G_{\rm F} n_\nu$ can lead to so-called slow flavor conversions, also known as bipolar pendulumlike oscillations [1,2] with rates $\sim(\omega\mu)^{1/2}$. These kind of collective oscillations can also lead to a swapping of the energy spectra of electron-type neutrinos with those of muon/taulike neutrinos at a specific critical energy [3–7], also known as spectral splits. Furthermore, it was pointed out by Sawyer [8,9] that small initial deviations from a pure flavor state can lead to so-called fast flavor conversions proceeding with characteristic rates of order μ. In the context of core collapse supernovae around and inside the neutrinosphere where neutrino nonforward interactions decouple, one typically has $\mu \gg \omega$ by several orders of magnitude such that fast flavor oscillations are in fact the most efficient. Through a linear stability analysis it was later shown that this effect is driven by a flip in sign of the local electron lepton minus muon/tau lepton number as function of the angle with respect to the radial direction (a so-called flavor-lepton number crossing) [10–12]. A particular difference between slow and fast conversions is that the basic version of the former can be described within ordinary differential equations in either time for a homogeneous system or in, for example, radial direction, for a stationary system, whereas the latter depend on propagating flavor waves which thus have to be described by partial differential equations. For some recent reviews see Ref. [13–15]. The fast collective flavor oscillations in particular are the subject of intense recent study, see, e.g., Refs. [16–19].

More recently, in attempts to make the analysis more and more realistic, more ingredients have been added and some simplifying assumptions such as certain symmetries have been dropped. For example, bipolar oscillations can be modified when the assumption of homogeneity is dropped and the system is described by partial differential equations [20]. While frequent nonforward scattering tends to damp neutrino oscillations [21] neutrino scattering off the ambient matter can lead to a neutrino halo even outside the neutrino sphere where nonforward scattering is rare. The influence of such a neutrino halo on the neutrino self-interactions has been investigated in Refs. [22,23]. The role of the convective terms in fast flavor conversions with inhomogeneous initial conditions with otherwise spatially homogeneous couplings have been investigated in Ref. [24]. In addition, the role of charged current source and sink terms for the neutrinos [25,26] as well as of nonforward neutral current collisions in

*guenter.sigl@desy.de

fast collective oscillations have been investigated [27,28]. Reference [29] found that in the presence of a sufficiently large asymmetry between interaction rates for neutrinos and antineutrinos a new kind of collisional instability can occur. Three-flavor effects have also been considered [30]. It turns out that most if not all of those ingredients can significantly modify the character of the resulting flavor conversions.

In the current study we do not attempt to perform a complete treatment in any sense, but to develop a numerical toy model setup that is at the same time simple enough to be run with reasonable resources and at the same time still sufficiently complex to study some of the effects mentioned above at least in a qualitative way. To this end we will solve a partial differential equation in one time and one (radial) dimension with a discrete number of momentum modes that has a Liouville-type transport term on the left hand side and a commutator describing vacuum, matter and collective oscillations as well as a collision term involving charged and neutral current term on the right hand side.

To mimic the situation in a core collapse supernova we then numerically solve these equations in particular in the context of radial profiles for the various rates. We investigate specifically the role of the matter oscillation term and the collision terms in the presence of profiles.

In Sec. II we describe the relevant general partial differential equation in 3 space and one time dimension with a continuum of momentum modes. In Sec. III we simplify this general equation to one time and one (radial) dimension with discrete momentum modes. In Sec. IV we then perform numerical simulations with this equation and present results for some cases of interest. Section V contains a discussion of the results and we conclude in Sec. VI.

II. KINETIC EQUATIONS FOR COLLECTIVE OSCILLATIONS

We consider N_f flavors of neutrinos and anti-neutrinos with annihilation operators a_i and b_i and creation operators $a_i^\dagger$ and $b_i^\dagger$, respectively, which act at a given location $\mathbf{r}$ or momentum $\mathbf{p}$. As dynamical variables we then use the corresponding Wigner distributions defined by

$$\begin{aligned}\rho_{ij}(\mathbf{r},\mathbf{p}) &\equiv \int d^3\mathbf{r}' e^{-i\mathbf{p}\cdot\mathbf{r}'}\langle a_j^\dagger(\mathbf{r}-\mathbf{r}'/2)a_i(\mathbf{r}+\mathbf{r}'/2)\rangle \\ &= \int \frac{d^3\mathbf{\Delta}}{(2\pi)^3} e^{i\mathbf{\Delta}\cdot\mathbf{r}}\langle a_j^\dagger(\mathbf{p}-\mathbf{\Delta}/2)a_i(\mathbf{p}+\mathbf{\Delta}/2)\rangle, \\ \bar\rho_{ij}(\mathbf{r},\mathbf{p}) &\equiv \int d^3\mathbf{r}' e^{-i\mathbf{p}\cdot\mathbf{r}'}\langle b_i^\dagger(\mathbf{r}-\mathbf{r}'/2)b_j(\mathbf{r}+\mathbf{r}'/2)\rangle \\ &= \int \frac{d^3\mathbf{\Delta}}{(2\pi)^3} e^{i\mathbf{\Delta}\cdot\mathbf{r}}\langle b_i^\dagger(\mathbf{p}-\mathbf{\Delta}/2)b_j(\mathbf{p}+\mathbf{\Delta}/2)\rangle, \end{aligned} \quad (1)$$

see, e.g., Ref. [31]. For a derivation and general discussion of the following kinetic equations see, e.g., Ref. [32]. We consider the equations of motion for these variables,

$$\begin{aligned}&\partial_t\rho(\mathbf{r},\mathbf{p}) + \mathbf{v}(\mathbf{r},\mathbf{p})\cdot\nabla_{\mathbf{r}}\rho(\mathbf{r},\mathbf{p}) \\ &= -i[\Omega^0_{\mathbf{p}} + \Omega_m(\mathbf{r}) + \Omega^{\mathrm{S}}(\mathbf{r},\mathbf{p}),\rho_{\mathbf{p}}] + \partial_t\rho(\mathbf{r},\mathbf{p})_{\mathrm{coll}}, \\ &\partial_t\bar\rho(\mathbf{r},\mathbf{p}) + \mathbf{v}(\mathbf{r},\mathbf{p})\cdot\nabla_{\mathbf{r}}\bar\rho(\mathbf{r},\mathbf{p}) \\ &= +i[\Omega^0_{\mathbf{p}} - \Omega_m(\mathbf{r}) - \Omega^{\mathrm{S}}(\mathbf{r},\mathbf{p}),\bar\rho_{\mathbf{p}}] + \partial_t\bar\rho(\mathbf{r},\mathbf{p})_{\mathrm{coll}}, \end{aligned} \quad (2)$$

where $[\cdot,\cdot]$ is the commutator,

$$\Omega_m \equiv \mathrm{diag}[\lambda_1(\mathbf{r}),\ldots,\lambda_n(\mathbf{r})], \quad (3)$$

is the in general space-dependent background matter contribution to the rotation frequency matrix which is diagonal in the flavor basis,

$$\Omega^0_{\mathbf{p}} \equiv \frac{1}{2p}\mathrm{diag}(m_1^2,\ldots,m_n^2), \quad (4)$$

is the matrix of vacuum oscillation frequencies, expressed in the mass basis, for ultrarelativistic neutrinos, with $p = |\mathbf{p}|$, and the self-interactions are characterized by

$$\begin{aligned}\Omega^{\mathrm{S}}(\mathbf{r},\mathbf{p}) = \sqrt{2}G_{\mathrm{F}}\int\frac{d^3\mathbf{q}}{(2\pi)^3}g_{\mathbf{p},\mathbf{q}}\{G_{\mathrm{S}}[\rho(\mathbf{r},\mathbf{q}) \\ -\bar\rho(\mathbf{r},\mathbf{q})]G_{\mathrm{S}} + G_{\mathrm{S}}\mathrm{Tr}[(\rho(\mathbf{r},\mathbf{q})-\bar\rho(\mathbf{r},\mathbf{q}))G_{\mathrm{S}}]\},\end{aligned} \quad (5)$$

where G_{F} is Fermi's constant, G_{S} is a dimensionless Hermitian matrix of coupling constants, which is just the unit matrix for active Standard Model neutrinos, and $g_{\mathbf{p},\mathbf{q}}$ are dimensionless momentum mode dependent coupling constants. With $\mathbf{v}_{\mathbf{p}}$ the neutrino velocity in momentum mode $\mathbf{p}$ it is generally given by $g_{\mathbf{p},\mathbf{q}} = 1 - \mathbf{v}_{\mathbf{p}}\cdot\mathbf{v}_{\mathbf{q}}$.

Furthermore, we schematically added a collision term $\partial_t\rho(\mathbf{r},\mathbf{p})_{\mathrm{coll}}$ on the right-hand side (rhs) of Eq. (2). It can have contributions from charged current source/sink terms of the form

$$\begin{aligned}\partial_t\rho(\mathbf{r},\mathbf{p})_{\mathrm{coll,CC}} &= \left\{\mathcal{P}(\mathbf{r},\mathbf{p}),\left(1-\frac{\rho(\mathbf{r},\mathbf{p})}{f_0(\mathbf{r},\mathbf{p})}\right)\right\}, \\ \partial_t\bar\rho(\mathbf{r},\mathbf{p})_{\mathrm{coll,CC}} &= \left\{\mathcal{A}(\mathbf{r},\mathbf{p}),\left(1-\frac{\bar\rho(\mathbf{r},\mathbf{p})}{\bar f_0(\mathbf{r},\mathbf{p})}\right)\right\}, \end{aligned} \quad (6)$$

with $f_0(\mathbf{r},\mathbf{p})$ and $\bar f_0(\mathbf{r},\mathbf{p})$ equilibrium occupation numbers in mode $\mathbf{p}$ and $\mathcal{P}(\mathbf{r},\mathbf{p})$ and $\mathcal{A}(\mathbf{r},\mathbf{p})$ some matrix-valued rates that we will specify later. Further contributions to the collision term can come from neutral current interactions which can be written as

$$\partial_t \rho(\mathbf{r},\mathbf{p})_{\text{coll,NC}} = \frac{1}{2}\int \frac{d^3\mathbf{q}}{(2\pi)^3}\{W(\mathbf{r},q,p)(1-\rho_\mathbf{p})G\rho_\mathbf{q}G - W(\mathbf{r},p,q)\rho_\mathbf{p}G(1-\rho_\mathbf{q})G + W(\mathbf{r},-q,p)(1-\rho_\mathbf{p})G(1-\bar{\rho}_\mathbf{q})G - W(\mathbf{r},p,-q)\rho_\mathbf{p}G\bar{\rho}_\mathbf{q}G + \text{H.c.}\},$$
$$\partial_t \bar{\rho}(\mathbf{r},\mathbf{p})_{\text{coll,NC}} = \frac{1}{2}\int \frac{d^3\mathbf{q}}{(2\pi)^3}\{W(\mathbf{r},-p,-q)(1-\bar{\rho}_\mathbf{p})G\bar{\rho}_\mathbf{q}G - W(\mathbf{r},-q,-p)\bar{\rho}_\mathbf{p}G(1-\bar{\rho}_\mathbf{q})G + W(\mathbf{r},-p,q)(1-\bar{\rho}_\mathbf{p})G(1-\rho_\mathbf{q})G - W(\mathbf{r},q,-p)\bar{\rho}_\mathbf{p}G\rho_\mathbf{q}G + \text{H.c.}\}, \quad (7)$$

where q and p are neutrino four momenta with positive energy $p_0 = |\mathbf{p}|$ and $q_0 = |\mathbf{q}|$, $W(\mathbf{r},q,p)$ are non-negative scattering rates per unit neutrino density and G is another dimensionless Hermitian matrix of coupling constants.

Generally the velocity of the neutrino $\mathbf{v}(\mathbf{r},\mathbf{p})$ depends on $\mathbf{r}$ and $\mathbf{p}$. Strictly speaking, the Liouville term on the left-hand side of Eq. (2) should read

$$\frac{1}{2}\{\nabla_\mathbf{r}\rho(\mathbf{r},\mathbf{p}),\nabla_\mathbf{p}\Omega(\mathbf{r},\mathbf{p})\} - \frac{1}{2}\{\nabla_\mathbf{p}\rho(\mathbf{r},\mathbf{p}),\nabla_\mathbf{r}\Omega(\mathbf{r},\mathbf{p})\} \quad (8)$$

and similarly for $\dot{\bar{\rho}}(\mathbf{r},\mathbf{p})$, where $\{.,.\}$ is the anticommutator. Here, $\Omega(\mathbf{r},\mathbf{p})$ is the matrix of total energies which includes external potentials like gravity as well as the refractive energy shifts discussed above. The latter are represented by the terms $\Omega^0_\mathbf{p} \pm \Omega_m(\mathbf{r}) \pm \Omega^S(\mathbf{r})$ in the commutators in Eq. (2). Therefore, the left-hand side of Eq. (2) would include a drift term proportional to the neutrino velocity $\mathbf{v} = \nabla_\mathbf{p}\Omega(\mathbf{r},\mathbf{p})$ and a term proportional to the force $\mathbf{F} = -\nabla_\mathbf{r}\Omega(\mathbf{r},\mathbf{p})$ acting onto the neutrino. However, we here neglect the force $\mathbf{F}$ and approximate $\mathbf{v}(\mathbf{r},\mathbf{p}) \simeq \mathbf{p}/E_\mathbf{p}$ and project it on a direction of interest. Furthermore, the velocities $\mathbf{v}_\mathbf{p}$ and the couplings $g_{\mathbf{p},\mathbf{q}} = 1 - \mathbf{v}_\mathbf{p}\cdot\mathbf{v}_\mathbf{q}$ could be made radius or time dependent to mimic the geometry of a supernova, for example.

The initial conditions can be parametrized as

$$\rho(t=0,\mathbf{r},\mathbf{p}) = \frac{n(\mathbf{r},\mathbf{p})}{2}\begin{pmatrix} 1+\cos\theta(\mathbf{r},\mathbf{p}) & \exp[i\phi(\mathbf{r},\mathbf{p})]\sin\theta(\mathbf{r},\mathbf{p}) \\ \exp[-i\phi(\mathbf{r},\mathbf{p})]\sin\theta(\mathbf{r},\mathbf{p}) & 1-\cos\theta(\mathbf{r},\mathbf{p}) \end{pmatrix}, \quad (9)$$

where the total occupation numbers $n(\mathbf{r},\mathbf{p})$ are fixed during evolution if nonforward scattering can be neglected and the initial polarizations are characterized by the angles $\theta(\mathbf{r},\mathbf{p})$ and $\phi(\mathbf{r},\mathbf{p})$. An analogous expression can be written for the initial antineutrino matrices.

A unique solution of the partial differential equations also requires to specify boundary conditions. We will adapt those to the specific problem we will consider in the next section.

III. NUMERICAL IMPLEMENTATION

In general we use $N_f = 2$ flavors, one spatial dimension x and a fixed number N_p of momentum modes and thus characterize $\rho(\mathbf{r},\mathbf{p})$ by $\rho(x,i_p)$ with a real spatial coordinate x in the range $0 \le x \le L$ and an integer i_p in the range $1 \le i_p \le N_p$. Furthermore, we set $G_S = \text{diag}(1,\ldots,1)$.

The N_p momentum modes cover velocities in the unique direction x within a range $v_{\min} \le v_x(i_p) \le v_{\max}$. All modes are assumed to have the same absolute value for the momentum, i.e., we only consider angular modes at a given absolute momentum $p = 1$.

For the vacuum oscillation terms in Eq. (2) we choose

$$\Omega^0_p = \frac{\Delta m^2}{4p}\begin{pmatrix} \cos 2\theta_0 & -\sin 2\theta_0 \\ -\sin 2\theta_0 & -\cos 2\theta_0 \end{pmatrix}, \quad (10)$$

in the flavor basis where θ_0 is the vacuum mixing angle and $\Delta m^2 = m_1^2 - m_2^2$. Thus, for $\theta_0 < \pi/4$ the inverted mass hierarchy corresponds to $\Delta m^2 > 0$. In the cases we will consider there is no momentum dependence because constant absolute momentum is considered. For the matter term we take

$$\Omega_m(x) = \lambda(x)\frac{1+\sigma_3}{2} = \lambda(x)\begin{pmatrix} 1 & 0 \\ 0 & 0 \end{pmatrix}, \quad (11)$$

with a scalar function $\lambda(x)$ that represents a rate that may depend on x.

To discretize the forward-scattering self-interaction term Eq. (5) is a bit more tricky. In principle one would substitute the momentum integral by a discrete sum $V^{-1}\sum_\mathbf{q}$ where V

is a quantization volume. Since we here effectively reduce the problem to a one-dimensional one and only take into account a small number of radial modes, we substitute $\sqrt{2}G_{\rm F}V^{-1}\sum_{\mathbf{q}} g_{\mathbf{p},\mathbf{q}}$ by $\mu(x)\sum_{i_q} g_{i_p,i_q}$. Here, $\mu(x)$ is an effective self-interaction rate of order $\sqrt{2}G_{\rm F}n_\nu(x)$ with $n_\nu(x)$ the neutrino density. The decrease of $\mu(x)$ with increasing x mimics the fact that in three dimensions, due to dilution in the transverse directions the neutrino density falls off faster than in the one-dimensional transport model used here. The coupling constants g_{i_p,i_q} are normalized such that the average of $\sum_{i_q} g_{i_p,i_q}$ over i_p is unity. For the toy scenarios below we use

$$g_{i_p,j_q} = \frac{(1-\delta_{i_p j_q})[1-v_x(i_p)v_x(j_q)]}{\sum_{i_k j_l}(1-\delta_{i_k j_l})[1-v_x(i_k)v_x(j_l)]/N_p}, \tag{12}$$

which assures that a given mode does not couple to itself and that the average coupling of one momentum mode summed over all other modes in Eq. (5) is unity and thus does not depend on N_p. With this we finally get

$$\Omega^{\rm S}(x,i_p) = \mu(x)\sum_{i_q\neq i_p} g_{i_p,i_q}\{G_{\rm S}[\rho(x,i_q)-\bar\rho(x,i_q)]G_{\rm S} + G_{\rm S}{\rm Tr}[(\rho(x,i_q)-\bar\rho(x,i_q))G_{\rm S}]\}. \tag{13}$$

For the charged current interaction term in one spatial dimension we use

$$\begin{aligned}\partial_t\rho(x,i_p)_{\rm coll,CC} &= f_{\rm CC}(x,i_p)\left\{\begin{pmatrix}1&0\\0&0\end{pmatrix}, \left(1-\frac{\rho(x,i_p)}{f_0(x,i_p)}\right)\right\},\\ \partial_t\bar\rho(x,i_p)_{\rm coll,CC} &= \bar f_{\rm CC}(x,i_p)\left\{\begin{pmatrix}1&0\\0&0\end{pmatrix}, \left(1-\frac{\bar\rho(x,i_p)}{\bar f_0(x,i_p)}\right)\right\},\end{aligned} \tag{14}$$

where $f_{\rm CC}(x,i_p)$, $\bar f_{\rm CC}(x,i_p)$, $f_0(x,i_p)$, and $\bar f_0(x,i_p)$ are suitably chosen functions. Equation (14) describes the injection of a pure flavor with a rate characterized by $f_{\rm CC}(x,i_p)$ and $\bar f_{\rm CC}(x,i_p)$ and equilibrium occupation numbers $f_0(x,i_p)$ and $\bar f_0(x,i_p)$.

For simplicity for the neutral current interactions we here neglect pair creation and annihilation terms out of and into the medium and assume that the rates $W(\mathbf{r},q,p)$ do not depend on q or p (isotropic, energy-independent scattering). Then the terms quadratic in ρ cancel and one can write

$$\partial_t\rho(x,i_p)_{\rm coll,NC} = f_{\rm NC}(x)\left\{\frac{1}{N_p}\sum_{i_q} G\rho(x,i_q)G - \frac{1}{2}[\rho(x,i_p)G^2 + G^2\rho(x,i_p)]\right\}, \tag{15}$$

where $f_{\rm NC}(x)$ is a location dependent scattering rate and we use $G = G_{\rm S}$. An analogous equation holds for antineutrinos. The scattering term is again normalized such that it does not depend on N_p.

Assuming isotropic energy-independent rates it is easy to see from Eq. (7) that one can include neutrino pair creation and pair annihilation out of and into the medium by generalizing Eq. (15) to

$$\partial_t\rho(x,i_p)_{\rm coll,NC} = f_{\rm NC}(x)\left\{\frac{1}{N_p}\sum_{i_q} G[\rho(x,i_q)-\bar\rho(x,i_q)]G - [\rho(x,i_p)G^2 + G^2\rho(x,i_p)] + G^2\right\}, \tag{16}$$

with an analogous equation for antineutrinos. This would, however, be only realistic for neutrino energies much smaller than the medium temperature because otherwise pair creation rates out of the medium would be thermally suppressed with respect to pair annihilation into the medium, which calls for a more detailed implementation which we postpone to future work. We will, therefore, use Eq. (15) throughout the present studies.

To model anisotropies and asymmetries between neutrinos and antineutrinos, let us now define

$$h(x,i_p) = \left(2\frac{i_p-1}{N_p-1}-1\right)g(x), \tag{17}$$

where $g(x)$ vanishes at the boundaries, $g(0) = g(L) = 0$. With this we also define the modulation factors

$$\begin{aligned} f(x,i_p) &= \frac{1}{2}[1-ah(x,i_p)][1-bh(x,i_p)],\\ \bar f(x,i_p) &= \frac{1}{2}[1-ah(x,i_p)][1+bh(x,i_p)],\end{aligned} \tag{18}$$

where a and b characterize the anisotropy in the neutrino plus antineutrino distribution $f(x,i_p)+\bar{f}(x,i_p)$ and the asymmetry between neutrinos and antineutrinos, respectively. Thus, since $h(x,i_p)$ vanishes at the spatial boundaries by construction, independent of the values for a and b we assume isotropy of the distribution at the boundaries within the chosen momentum range. Also note that $a=b=0$ corresponds to an isotropic distribution everywhere in which case $h(x,i_p)$ is irrelevant. Based on these definitions we now set equilibrium occupation numbers, injection rates, and initial conditions proportional to $f(x,i_p)$ and $\bar{f}(x,i_p)$ with x–dependent normalizations that can be suitably chosen. The equilibrium occupation numbers then become

$$f_0(x,i_p)=f_0(x)f(x,i_p),\quad \bar{f}_0(x,i_p)=f_0(x)\bar{f}(x,i_p), \tag{19}$$

where $f_0(x)$ represents an overall normalization, and the injection rates are

$$f_{\rm CC}(x,i_p)=f_s(x)f(x,i_p),\qquad \bar{f}_{\rm CC}(x,i_p)=f_s(x)\bar{f}(x,i_p), \tag{20}$$

where $f_s(x)$ again represents an overall normalization. Note that this ansatz ensures that any initial anisotropy and/or neutrino/antineutrino asymmetry is supported by these source terms.

For the initial condition Eq. (9) we use

$$\begin{aligned}\rho(t=0,x,i_p)&=f_i(x)f(x,i_p)M(x),\\ \bar{\rho}(t=0,x,i_p)&=f_i(x)\bar{f}(x,i_p)M(x),\end{aligned} \tag{21}$$

where the x–dependent $f_i(x)$ characterizes the total neutrino plus antineutrino occupation number and the matrix M is parametrized as

$$M(x)=\frac{1}{2}\begin{pmatrix}1+\cos\theta(x) & \exp[i\phi(x)]\sin\theta(x)\\ \exp[-i\phi(x)]\sin\theta(x) & 1-\cos\theta(x)\end{pmatrix}. \tag{22}$$

We will typically use random numbers for the angles $\theta(x)$ and $\phi(x)$, with a characteristic (small) amplitude A for $\theta(x)$. This assures that initially the flavor state will be close to the dominant flavor 1, which in the supernova context typically are electron neutrinos.

The ansatz Eq. (21) with Eq. (18) assures that for $b\neq 0$ the lepton number of flavor 1 exhibits a flip of sign within the momentum range simulated or, more generally, the lepton number asymmetry as a function of the unit vector $\mathbf{n}$ characterizing the direction

$$\begin{aligned}G(\mathbf{r},\mathbf{n})=\int_0^\infty\frac{dpp^2}{2\pi^2}[&\rho_{11}(\mathbf{r},p\mathbf{n})-\bar{\rho}_{11}(\mathbf{r},p\mathbf{n})\\ &-\rho_{22}(\mathbf{r},p\mathbf{n})+\bar{\rho}_{22}(\mathbf{r},p\mathbf{n})],\end{aligned} \tag{23}$$

changes sign as a function of $\mathbf{n}$. This is known to be the criterion for fast flavor conversions to occur [10,33].

Note that the ansatze above imply that there is no global asymmetry between neutrinos and antineutrinos. The parameter b in Eq. (18) only leads to a local asymmetry in momentum which averages out when summing over all momenta. One could of course generalize this to a global asymmetry between neutrinos and antineutrinos by choosing some or all of the normalizations $f_0(x)$, $f_s(x)$ and $f_i(x)$ different for neutrinos and antineutrinos.

IV. RESULTS FOR SPECIFIC TOY MODELS

We here have in mind the situation of a core collapse supernova in which x represents the radial coordinate and the inner boundary at $x=0$ lies inside the neutrino decoupling sphere at high densities, whereas the outer boundary at $x=L$ lies outside the neutrino sphere at low densities. We apply angular modes covering $-1\leq v_x\leq 1$, with central values

$$v_x(i_p)=-1+\frac{1}{N_p}+\frac{i_p-1}{N_p-1}\left(2-\frac{2}{N_p}\right),\qquad i_p=1,\ldots,N_p, \tag{24}$$

with N_p even. In the following we will sometimes label the momentum modes with v_x instead of with i_p. At the outer boundary at $x=L$ the boundary condition for the incoming modes, $v_x<0$, is then simply chosen as fixed by the initial condition Eq. (21),

$$\begin{aligned}\rho(t,x=L,v_x<0)&=\rho(t=0,x=L,v_x<0)\\ \bar{\rho}(t,x=L,v_x<0)&=\bar{\rho}(t=0,x=L,v_x<0).\end{aligned} \tag{25}$$

The rationale is that there are very few incoming neutrinos at the outer boundary due to rare scattering and they are of the dominant flavor 1. The boundary conditions at $x=0$ are instead given in terms of a reflective boundary,

$$\begin{aligned}\rho(t,x=0,v_x)&=\rho(t,x=0,-v_x),\\ \bar{\rho}(t,x=0,v_x)&=\bar{\rho}(t,x=0,-v_x).\end{aligned} \tag{26}$$

Since at $x=0$ there is no momentum dependence for the initial conditions Eq. (21) because $f(x=0,i_p)=g(x=0)=0$, this is consistent with the initial conditions for arbitrary values of a and b. Here the rationale is that in

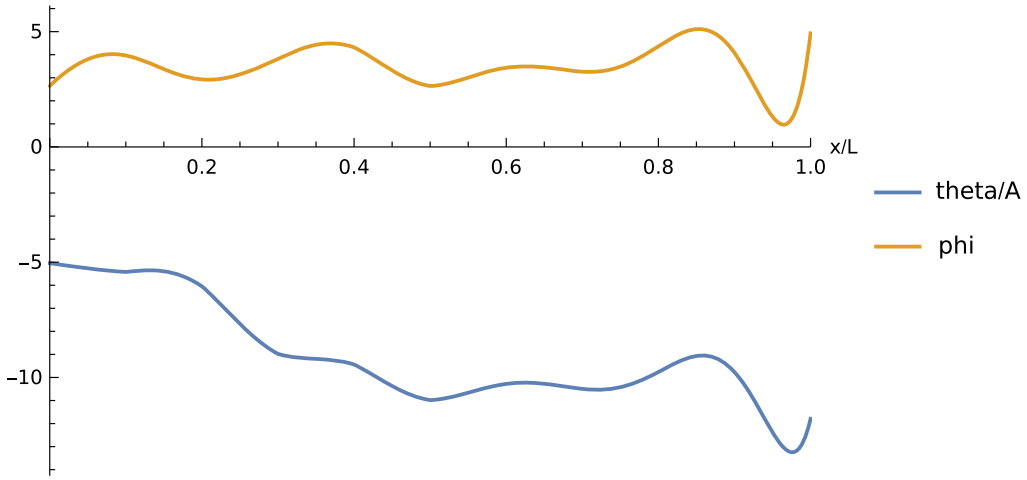

FIG. 1. The angles $\theta(x)$ and $\phi(x)$ in the initial conditions in Eq. (22) that we obtain from a random Wiener process. The angle $\theta(x)$ is multiplied with the amplitude $A = 10^{-5}$.

the high density region the distribution should be essentially isotropic due to frequent scattering.

In our simulations the total number of neutrinos at a given location and time is then given by

$$N(t,x) \equiv \sum_{v_x} \mathrm{Tr}[\rho(x,v_x) + \bar{\rho}(x,v_x)]. \tag{27}$$

Note that Eqs. (18) and (21) imply that $N(t=0,x) = N_p f_i(x)$ initially because $\sum_{i_p=1}^{N_p} h(x,i_p) = 0$ for $h(i_p)$ given by Eq. (17). With Eq. (27) we also define the normalized off-diagonal elements as

$$F_{\mathrm{off}}(t,x) \equiv \frac{\sum_{v_x} |\rho_{12}(x,v_x) + \bar{\rho}_{12}(x,v_x)|}{N(t,x)}, \tag{28}$$

and the normalized flavor asymmetry of the outgoing neutrino modes as

TABLE I. Summary of scenarios simulated. Here, L is the box size in the spatial coordinate, x_0 is the scale height of the exponential profiles, Δm^2 and θ_0 are the vacuum mixing parameters, $\mu(x)$ is the self-interaction strength, $\lambda(x)$ is the matter term and $f_{\mathrm{NC}}(x)$ is the normalization of the neutral current interactions. The initial conditions can have an electron lepton number crossing (ELNC) with $a = 0$, $b = 0.5$ in Eq. (18), where $g(x) = \sin(\pi x/L)\exp(-x/x_0)$ in Eq. (17) and random angles $\theta(x)$ and $\phi(x)$ as described in Eqs. (21) and (22) and shown in Fig. 1 with amplitude $A = 10^{-4}$, or they can represent an initially pure flavor 1 state in case (8). The boundary condition is usually reflective at $x = 0$, in which case at $x = L$ it is given by the initial condition for the incoming modes $v_x < 0$. For comparison, cases (9) and (10) represent the homogeneous case without profile and periodic boundary conditions. In this case the initial conditions are given by $g(x) = 1 + 0.1\sin(\pi x/L)$ in Eq. (17) and $\theta(x) = 10^{-5}$, $\phi(x) = 1.5$ in Eq. (22). The equilibrium and initial occupation numbers are $f_0(x) = \bar{f}_0(x) = f_i(x) = 0.8\exp(-x/x_0)$ and charged current interaction normalization is $f_s(x) = 0.1\exp(-x/x_0)$ for all simulations.

	Fig.	L, x_0	Δm^2, θ_0	$\mu(x)$	$\lambda(x)$	$f_{\mathrm{NC}}(x)$	Initial	Boundary
1	2	200, 100	0,0	$50\exp(-x/100)$	0	0	ELNC random	Reflective at $x = 0$
2	3	200, 100	0,0	$50\exp(-x/100)$	$50\exp(-x/100)$	0	ELNC random	Reflective at $x = 0$
3	4	200, 100	0,0	$50\exp(-x/100)$	50	0	ELNC random	Reflective at $x = 0$
4	5	500, 250	0,0	$50\exp(-x/250)$	0	0	ELNC random	Reflective at $x = 0$
5	6	500, 250	0,0	$50\exp(-x/250)$	$50\exp(-x/250)$	0	ELNC random	Reflective at $x = 0$
6	7	500, 250	0,0	$50\exp(-x/250)$	0	$0.1\exp(-x/250)$	ELNC random	Reflective at $x = 0$
7	8	500, 250	0,0	$50\exp(-x/250)$	$50\exp(-x/250)$	$\exp(-x/250)$	ELNC random	Reflective at $x = 0$
8	10	500, 250	0.1, 10^{-4}	$50\exp(-x/250)$	0	0	Pure flavor 1	Reflective at $x = 0$
9	11	500, ∞	0,0	50	0	0	ELNC, nonrandom	Periodic
10	12	500, ∞	0,0	50	0	0.1	ELNC, nonrandom	Periodic

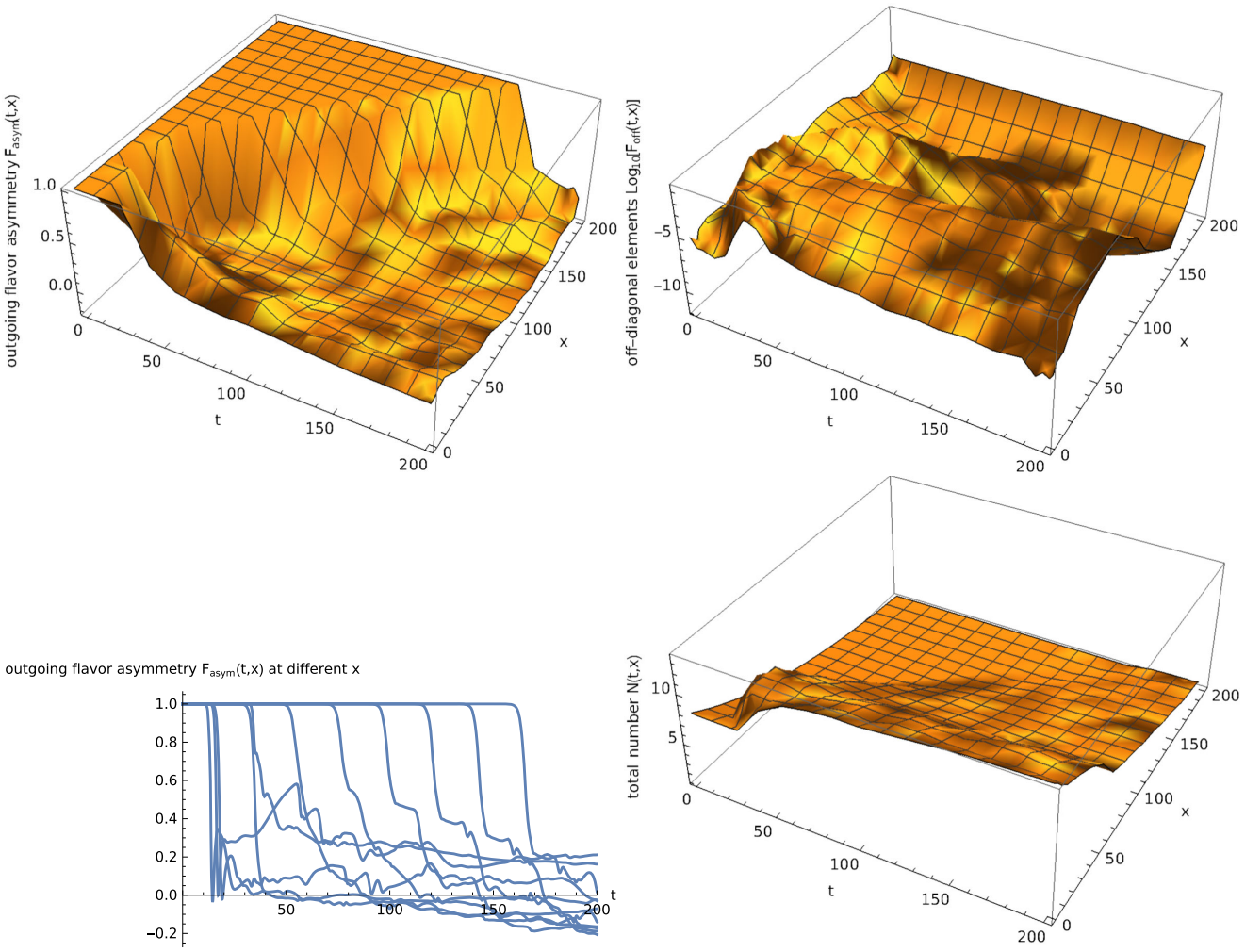

FIG. 2. Results for a case (1) simulation with $N_p = 10$ angular modes uniformly distributed in the range $0 \le v_x \le 1$, with initially, at $t = 0$, neutrinos and antineutrinos of mostly flavor 1 of total number $N(t = 0, x) = N_p f_i(x) = 0.8 N_p \exp(-x/100)$. For $0 < x < 200 = L$ random small deviations from a pure flavor 1 state have been chosen, as described in the text. The total initial anisotropy is assumed to vanish, $a = 0$, whereas a flavor crossing with $b = 0.5$ was used Eq. (18). Further, there is no vacuum term and $\mu(x) = 50 \exp(-x/100)$, $\lambda(x) = 0$, with integration up to $t = 200$. The charged current rates are proportional to $0.1 \exp(-x/100)$, whereas there is no neutral current scattering. Upper left: normalized flavor asymmetry of outgoing modes defined in Eq. (29). Upper right: normalized off-diagonal elements defined in Eq. (28). Lower left: cuts through flavor asymmetry from upper left at at 11 equidistant positions x between $x = 0$ and $x = 200$. Lower right: total number defined in Eq. (27).

$$F_{\rm asym}(t,x) \equiv \frac{\sum_{v_x>0}[\rho_{11}(x,v_x) - \rho_{22}(x,v_x) + \bar{\rho}_{11}(x,v_x) - \bar{\rho}_{22}(x,v_x)]}{\sum_{v_x>0}{\rm Tr}[\rho(x,v_x) + \bar{\rho}(x,v_x)]}. \tag{29}$$

We here restrict to the outgoing modes because those are the ones that in the end are observable and their occupation is not fixed by the boundary condition at the outer boundary.

Apart from the length L of the simulated range in x we specify a length scale x_0 on which the x–dependent functions in our problem vary. For the x–dependence of the modulation in Eqs. (17) and (18) we then generally use $g(x) = \sin(\pi x/L)\exp(-x/x_0)$, assuring $g(0) = g(L) = 0$. For the normalization of the equilibrium occupation numbers in Eq. (19) we choose $f_0(x) = \bar{f}_0(x) = 0.8\exp(-x/x_0)$, as well as for the normalization $f_i(x) = 0.8\exp(-x/x_0)$ of the initial occupation numbers in Eq. (21). For the normalization of the charged current

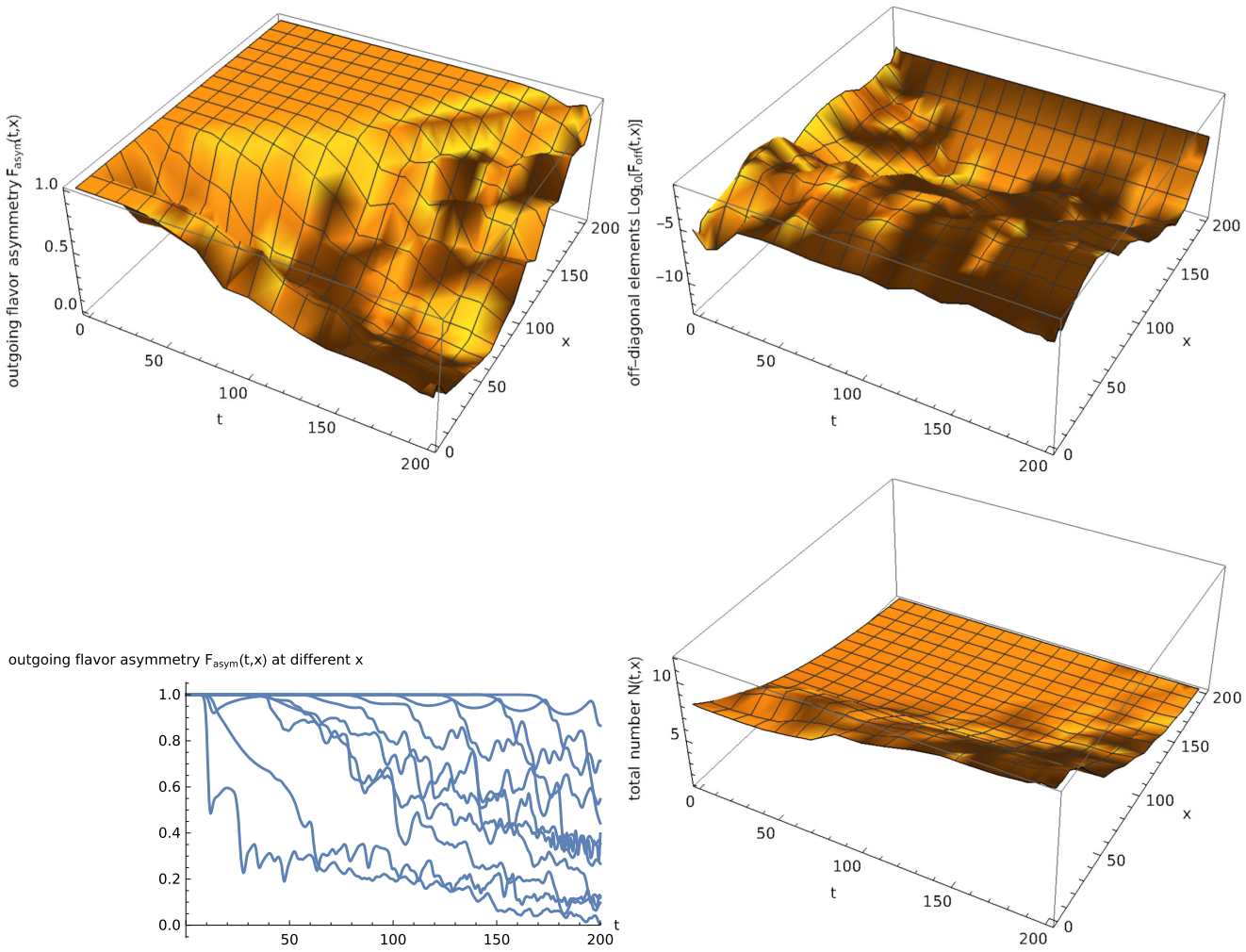

FIG. 3. Results for a case (2) simulation which is identical to case (1) but with an additional matter term $\lambda(x) = \mu(x) = 50\exp(-x/100)$. Note that the matter term partially suppresses and delays the flavor transitions.

rates in Eq. (20) we choose $f_s(x) = 0.1\exp(-x/x_0)$. The same exponential profiles are used for the matter and self-interaction terms, $\lambda(x) = \lambda_0\exp(-x/x_0)$, $\mu(x) = \mu_0\exp(-x/x_0)$.

Since we will here concentrate on fast flavor oscillations which do not depend on the vacuum term and the vacuum term in a type II supernova is generally much smaller than the matter and self-interaction terms, we here neglect it by putting $\Omega^0_{\mathbf{p}} = 0$ in Eq. (2) in most cases below.

To trigger flavor oscillations then requires small deviations from a pure flavor state as initial condition. For this we take a random Wiener process between $x = 0$ and $x = L$ for the angles in Eq. (22). The result is shown in Fig. 1 where for the amplitude for $\theta(x)$ we take $A = 10^{-4}$. This assures that initially the flavor state is very close to the dominant flavor 1. A flavor-lepton number crossing with amplitude $b = 0.5$ has been chosen in Eq. (18) at $t = 0$, whereas $a = 0$, and thus no global anisotropy, has been assumed initially. This flavor number crossing, together with its shape at later times, will be shown further below in Fig. 9.

In a supernova setting the various rates have the hierarchy $\lambda(x) \gtrsim \mu(x) \gg f_s(x) \simeq f_{\rm NC}(x)$. In order to mimic this situation our parameter value choices will reflect this hierarchy.

We generally used $N_p = 10$ and verified that for $N_p \gtrsim 10$ the results do not depend significantly on the number of angular modes N_p any more. The simulations are performed with *Mathematica* 12.1. A minimum of 10^4 steps is taken; i.e., for a range of 500 in x and t, one step has a length of at most 0.05 which is comparable to or

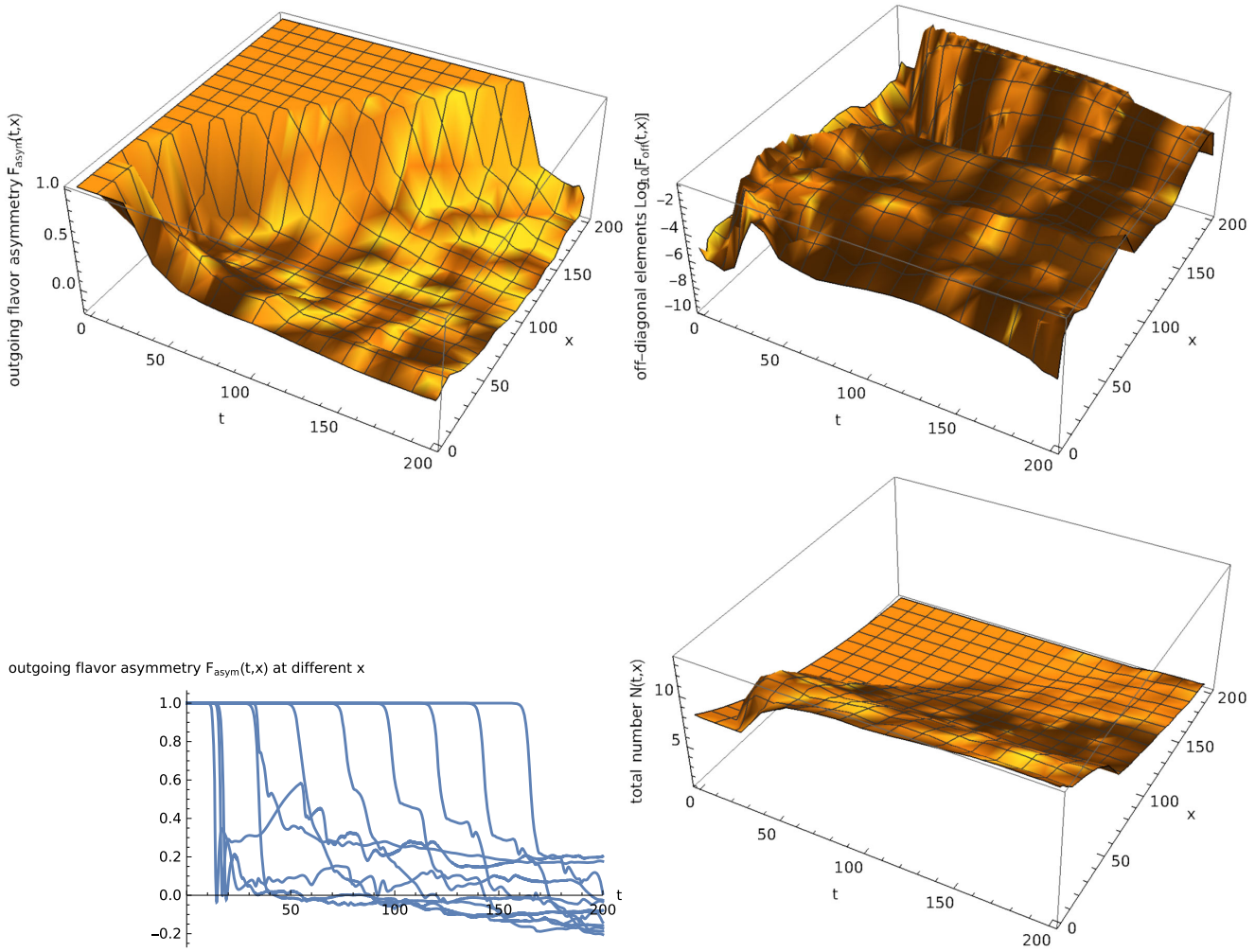

FIG. 4. Results for a case (3) simulation which is identical to case (1) but with an additional homogeneous matter term $\lambda(x) = 50$. Note that the matter term here has no discernible influence on the flavor evolution as the result for quantities depending on flavor-diagonal terms is virtually identical to case (1) shown in Fig. 2, as expected on theoretical grounds, see Sec. V. However, the off-diagonal terms shown in the upper right figure are in fact different from case (1).

smaller than the inverse of the fastest local rates. Furthermore the mathematica routine is auto-adaptive, so that the time steps can be much smaller in regions of large rates.

The cases that have been simulated are summarized in Table I. In the following we discuss them in more detail.

In case (1) shown in Fig. 2 we use $L = 200$, $x_0 = 100$, a self-interaction rate $\mu(x) = 50\exp(-x/100)$, no matter term, $\lambda(x) = 0$, and no neutral current scattering terms, $f_{\mathrm{NC}}(x) = 0$. Case (2) shown in Fig. 3 is identical to case (1) except that there is a matter term $\lambda(x) = \mu(x) = 50\exp(-x/100)$. Case (3) has instead a homogeneous matter term $\lambda(x) = 50$. We also checked that choosing a constant $\mu(x) = 50$ instead of the profile does not change the results substantially.

Next we investigate the influence of neutral current scattering and the interplay with matter terms. To this end we use a shallower profile, $x_0 = 250$ with $L = 500$. Case (4) shown in Fig. 5 is identical to case (1) apart from these changes. In case (5) shown in Fig. 6 we add a matter term $\lambda(x) = \mu(x) = 50\exp(-x/100)$, whereas in case (6) shown in Fig. 7 we have a neutral current scattering term with $f_{\mathrm{NC}}(x) = 0.1\exp(-x/250)$ in Eq. (15) instead. Finally, case (7) shown in Fig. 8 combines a matter term $\lambda(x) = \mu(x) = 50\exp(-x/100)$ with a neutral current scattering term with normalization $f_{\mathrm{NC}}(x) = \exp(-x/250)$.

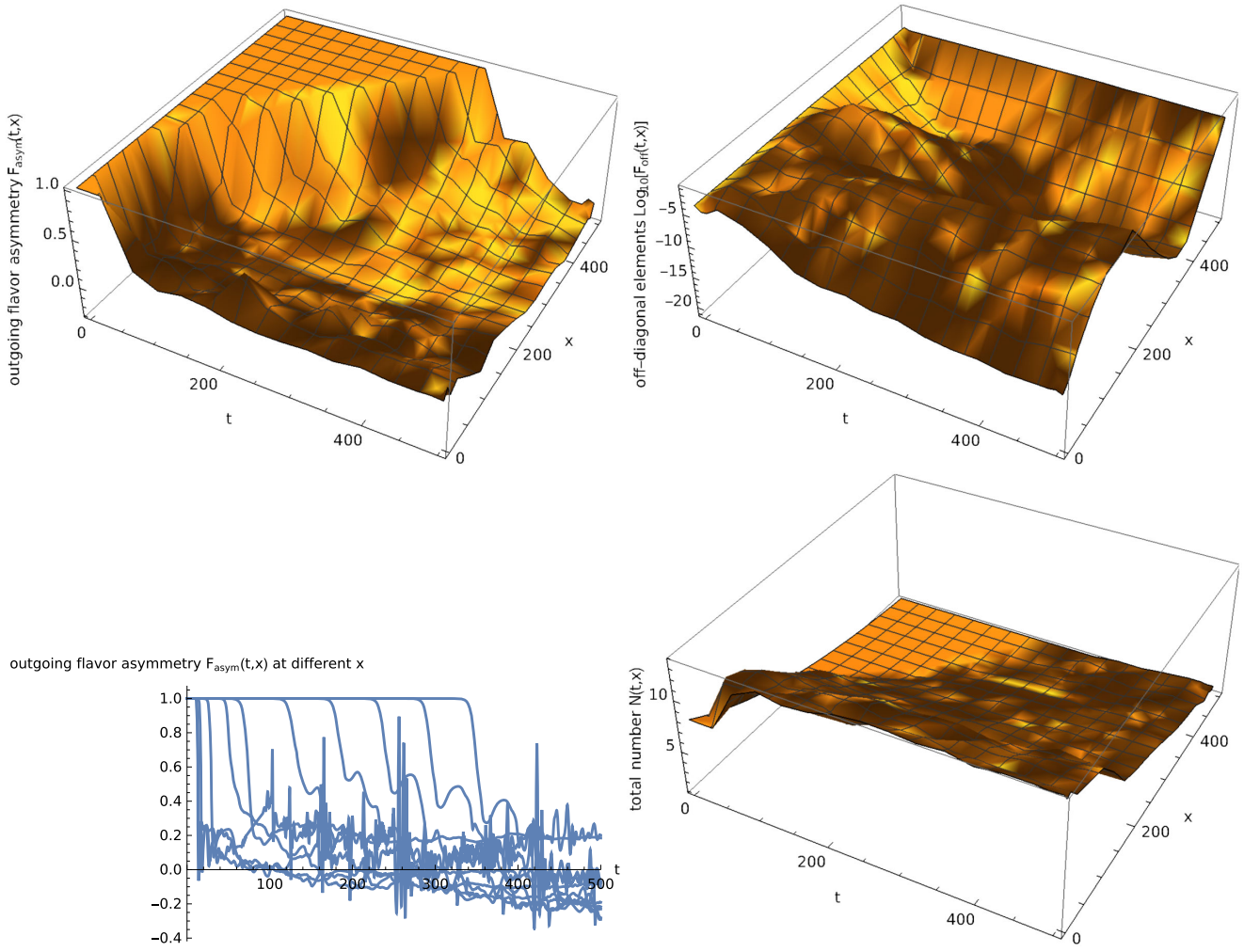

FIG. 5. Results for a case (4) simulation which is very similar to case (1) shown in Fig. 2, except for shallower profiles $\propto \exp(-x/250)$.

In Fig. 9 we plot the normalized flavor-lepton number asymmetry corresponding to Eq. (23),

$$G(t,x,v_x) \equiv \frac{\rho_{11}(x,v_x) - \rho_{22}(x,v_x) - \bar{\rho}_{11}(x,v_x) + \bar{\rho}_{22}(x,v_x)}{N(t,x)}, \tag{30}$$

as a function of direction $v_x = \cos\theta$ for cases (4) to (7), at several values for t and x. We see that both the matter term and the neutral current scattering term tend to suppress the initial asymmetry already at early times which leads to suppressed or delayed flavor conversions.

In case (8) we consider for comparison a scenario corresponding to so-called "slow" flavor conversions. In this case, we start with initial conditions for a pure flavor 1, $A = 0$, and thus $M(x) = \mathrm{diag}(1,1)$ in Eqs. (21) and (22), and no flavor-lepton number crossing, $b = 0$, in Eq. (18). The flavor conversions are instead triggered by a nonvanishing vacuum term with $\Delta m^2 = 0.1$, $\theta_0 = 10^{-4}$, i.e., an inverted hierarchy with a small vacuum mixing angle. All other parameters are as in case (4). The results are shown in Fig. 10.

Finally, to illustrate the role of profiles adopted in cases (1) through (8), in cases (9) and (10) we simulate a homogeneous situation with $\mu(x)050$, $\lambda(x) = 0$, and periodic boundary conditions. For compatibility with the periodic boundaries, for the initial conditions we choose constant $\theta(x) = 10^{-4}$, $\phi(x) = 1.5$ in Eq. (22) with a small modulation $g(x) = 1 + 0.1\sin(\pi x/L)$ of the normalization in Eq. (17). Case (9) shown in Fig. 11 has no neutral scattering, $f_{\mathrm{NC}}(x) = 0$, whereas case (10) shown in Fig. 12 has $f_{\mathrm{NC}}(x) = 0.1$.

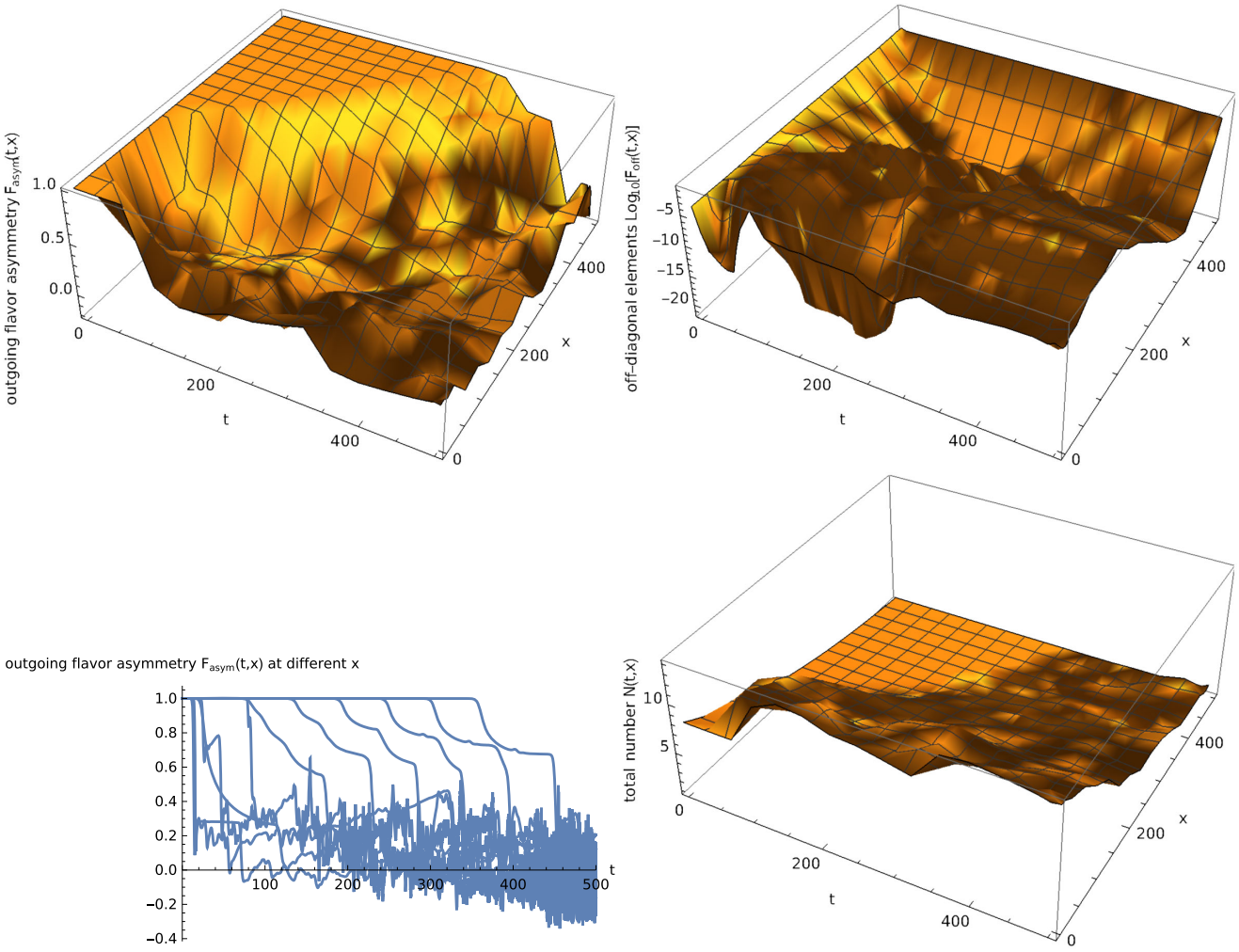

FIG. 6. Results for a case (5) simulation which is identical to case (4) but with an additional matter term $\lambda(x) = \mu(x) = 50\exp(-x/250)$. Note that the matter term partially suppresses and delays the flavor conversions.

In the following section we discuss these results in more detail.

V. DISCUSSION AND OUTLOOK

Let us first mention a few general aspects. It can be seen in the lower right panels of Figs. 2–8 that conversions from the originally dominating flavor 1 locally leads to an increase of the number of neutrinos, or neutrino density, at moderate radii. This is easy to understand since a decrease of flavor 1 occupation numbers leads to production of flavor 1 states by the charged current interactions. On the other hand, at large radii, close to the outer boundary, the neutrino density changes at most due to additional neutrinos produced in the inner region streaming outward. This is because at large radii the charged current interactions are too small to significantly change the neutrino number. Thus, the range of radii simulated in our examples indeed effectively covers regions within and outside the neutrino sphere.

The momentum sum of the off-diagonal terms shown in the upper right panels of Figs. 2–8 typically show a rise in the regions where flavor conversions take place, but tend to get strongly suppressed in regions where no collective oscillations happen, as one would expect. An exception is the outer boundary at $x = L$ where the off-diagonal components summed over all momenta (in- as well as outgoing) are essentially fixed by the boundary condition for modes propagating inwards Eq. (25) which equals the initial condition of flavor states close to flavor 1. This implies that the outgoing modes have very small off-diagonal elements, probably because they are averaged out by the oscillations and convective transport. Note that the upper left panels of Figs. 2–8 show the flavor asymmetry of only the outgoing modes, see Eq. (29),

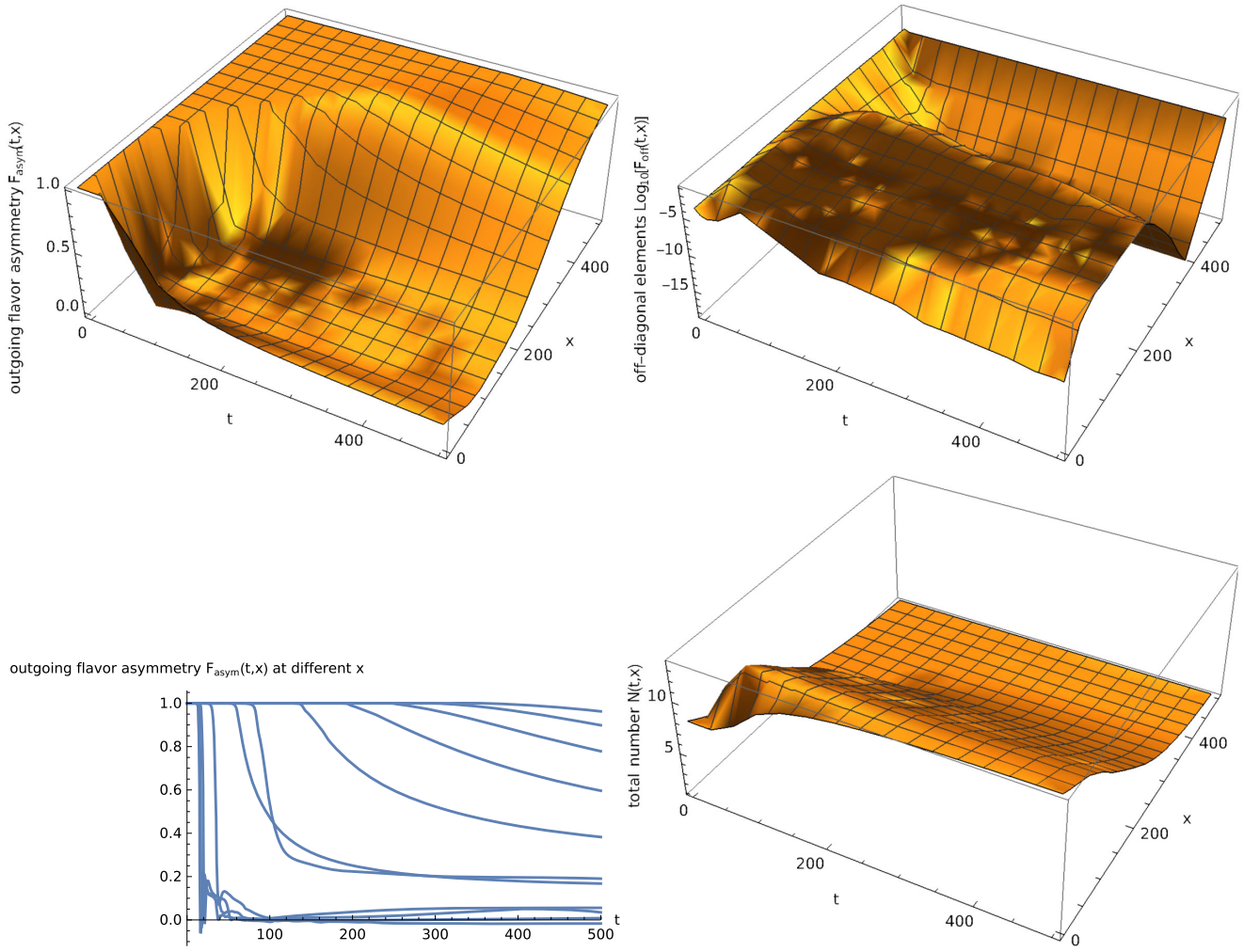

FIG. 7. Results for a case (6) simulation which is identical to case (4) but with an additional neutral current scattering term $\propto f_{\rm NC}(x) = 0.1\exp(-x/250)$. Note that the neutral current scattering term partially suppresses and delays the flavor conversions.

whereas the off-diagonal elements shown in the upper right panels are summed over all modes, see Eq. (28). Also note that efficient fast flavor conversions always saturate near flavor equilibration.

Using stability analysis for linear perturbations in a homogenous system characterized by $\mu \equiv \mu(x) = \text{const}$ one can show that fast flavor conversion instabilities occur for

$$|k_x|, \qquad \frac{1}{\sigma} < k_c \simeq \frac{4\mu b}{|v_1 - v_2|}, \tag{31}$$

and with a growth rate

$$R \simeq 2\mu b, \tag{32}$$

see, e.g., Ref. [14]. The results shown in Figs. 2–6 appear roughly consistent with this in the linear growth phase when substituting $\mu(x)bg(x) \simeq \mu_0 \sin(\pi x/L)\exp(-2x/x_0)$ for μb. Note that the effective conversion rates are larger around $x = 0$ compared to around $x = L$ due to the exponential factor. This explains why transitions first occur around $x = 0$. Later, transitions also occur around $x = L$, both due to the smaller rates and the convection from regions with higher conversion rates.

For case (8) for an initially pure flavor with non-vanishing vacuum terms shown in Fig. 10 one expects growth rates of the order of $[2\mu(x)\Delta m^2/(4p)]^{1/2} \sim 1$ [1] which is not much smaller than the "fast" transition rates discussed above, in particular on the timescales shown in Fig. 10. Still, in contrast to the other cases of "fast" transitions one can see bipolar oscillations at small times

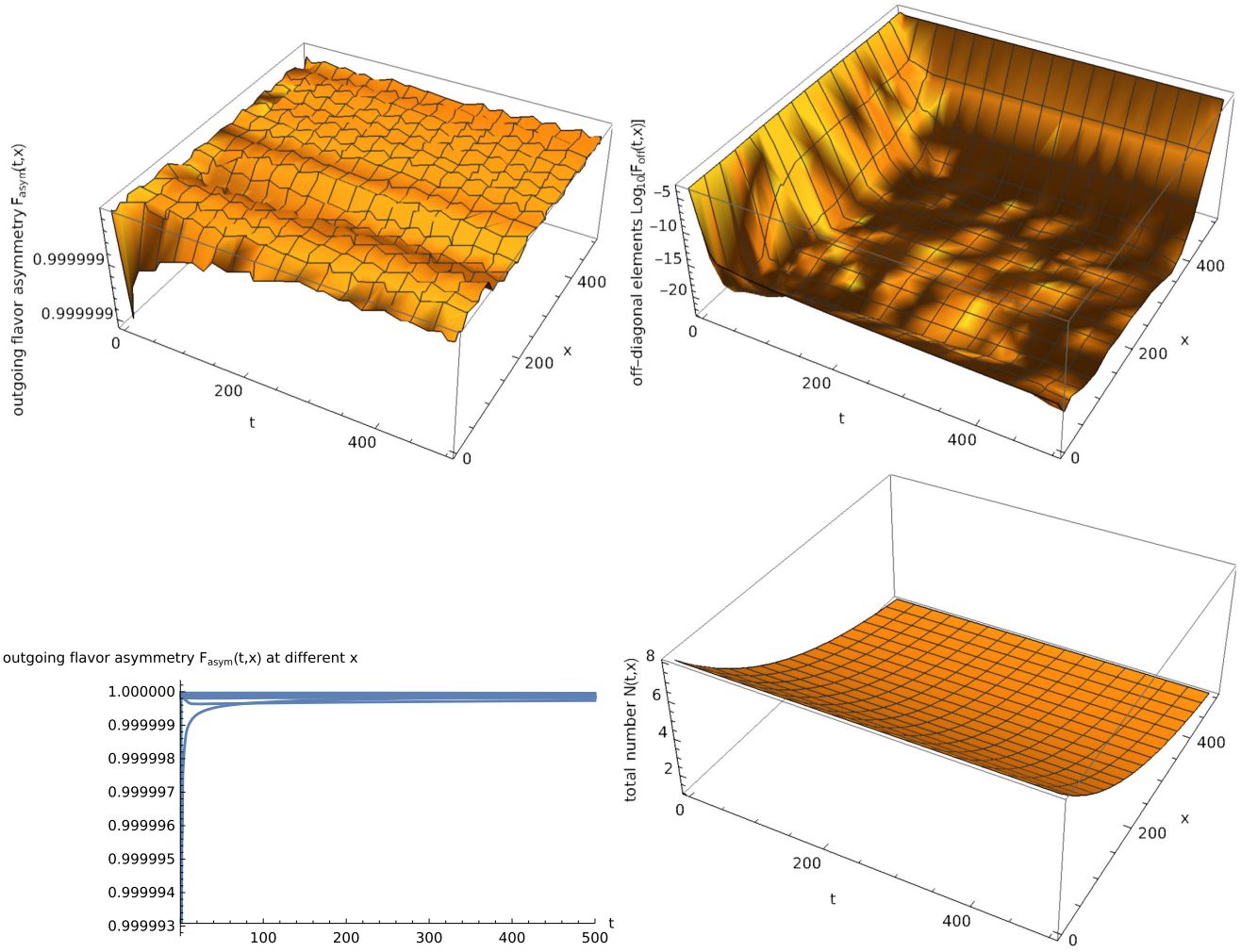

FIG. 8. Results for a case (7) simulation which is identical to case (4) but with an additional matter term $\lambda(x) = \mu(x) = 50\exp(-x/250)$ and an additional neutral current scattering term $\propto f_{\rm NC}(x) = \exp(-x/250)$. Note that the flavor conversions are completely suppressed in this case.

in which the flavor asymmetry goes considerably below zero, which makes it qualitatively different.

Comparing Figs. 2–10 for the cases (1)–(8) with exponential profiles with the homogeneous cases (9) and (10) with periodic boundary conditions shown in Figs. 11 and 12 shows that profiles have a strong influence on the spatial and time distributions of flavor conversions: Clearly, through the interplay between space-varying rates and the convection term the presence of profiles leads to a nontrivial structure of conversions in space and time which is not seen in the homogeneous case.

Furthermore, the upper left panels of Figs. 2–8 show that both neutral current scattering terms and refractive effects from the matter tend to partially suppress or at least delay the flavor conversions. Let us now discuss the role of these two ingredients in more detail.

In general, if the matter term in Eq. (3) is independent of the spatial coordinates, $\Omega_m(\mathbf{r}) = \lambda D$ with D a constant diagonal matrix with order unity entries and λ a constant rate, one can define modified density matrices through

$$\tilde{\rho}(t,\mathbf{r},\mathbf{p}) \equiv \exp\left[+i\lambda D t\right]\rho(t,\mathbf{r},\mathbf{p})\exp\left[-i\lambda D t\right], \qquad (33)$$

and an analogous equation for $\tilde{\bar{\rho}}(t,\mathbf{r},\mathbf{p})$ for the antineutrinos. Since D commutes with Ω_m, $G_{\rm S}$, G and the charged current matrix rates $\mathcal{P}(\mathbf{r},\mathbf{p})$ and $\mathcal{A}(\mathbf{r},\mathbf{p})$ in Eq. (6), it is easy to see that if $\rho(t,\mathbf{r},\mathbf{p})$ and $\bar{\rho}(t,\mathbf{r},\mathbf{p})$ obey Eq. (2), then $\rho(t,\mathbf{r},\mathbf{p})$ and $\tilde{\bar{\rho}}(t,\mathbf{r},\mathbf{p})$ also obey Eq. (2) but without the matter term Ω_m, as long as there is no off-diagonal vacuum term $\Omega^0_{\mathbf{p}}$ with which D does not

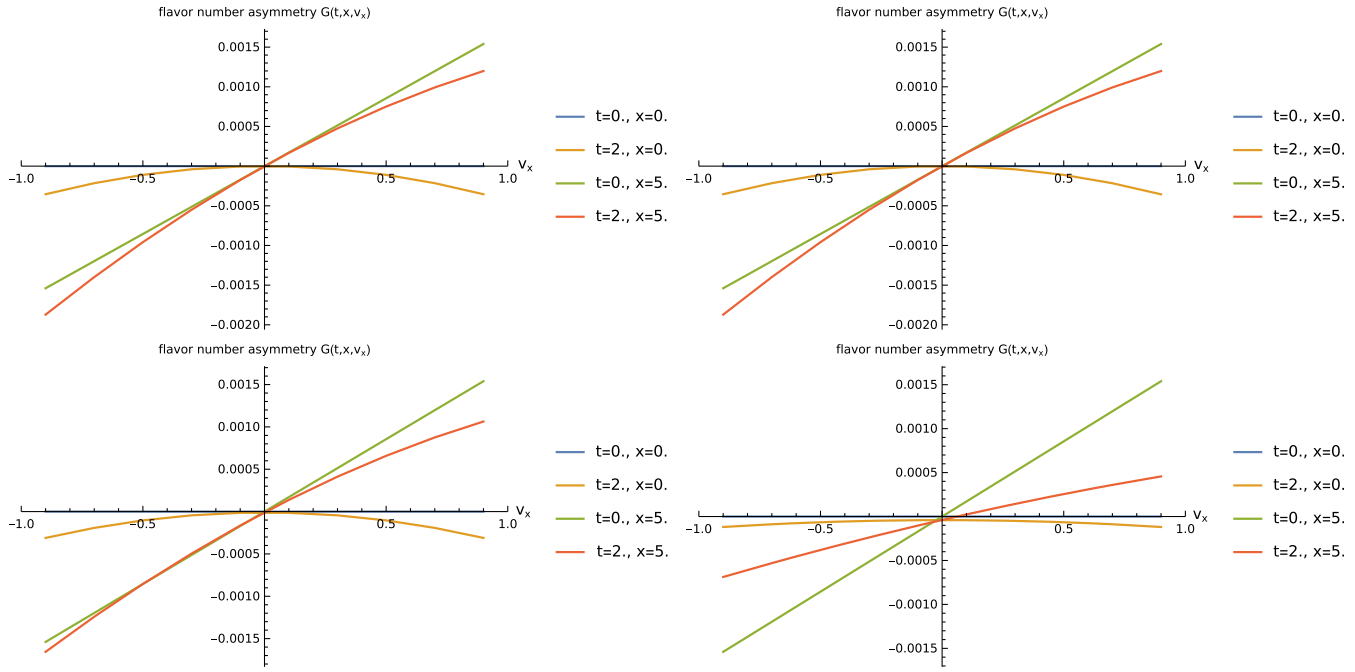

FIG. 9. The normalized flavor-lepton number asymmetry defined in Eq. (30) as a function of direction v_x for cases (4) (upper left), (5) (upper right), (6) (lower left) and (7) (lower right), at the values for t and x indicated. Note that at $t = 0$ the flavor-lepton number asymmetry is of order $bg(x)/N_p$ which for $x = 5$ gives $G(t = 0, x = 5, v_x) \simeq 0.00154 v_x$. At $x = L/2$ (not shown) the initial flavor asymmetry becomes maximal, $G(t = 0, x = L/2, v_x) \simeq 0.018 v_x$. Note that both the matter term and the neutral current scattering term tend to suppress the asymmetry already at early times.

commute. In this sense it is often said that the matter term is "rotated away" and thus effectively eliminated from the problem as long as one is mostly interested in the diagonal (flavor) content of the density matrices, see, e.g., Ref. [14]. This is confirmed by a comparison of cases (1) and (3) shown in Figs. 2 and 4, respectively. The influence of a homogeneous matter term is very small even in the presence of vacuum terms as long as the matter term is much larger than the vacuum term, $\lambda \gg \Delta m^2/(2p)$, whose off-diagonal components then tend to average out [2].

We note that some works in the literature did find an influence of even a constant matter term on collective oscillations. For example, in Ref. [34] it was found that electron densities larger than the neutrino densities can lead to multiangle decoherence which tends to suppress collective flavor conversions. Given the above analytical argument this may seem surprising, however those findings have usually been made assuming stationary solutions which turns the problem into an ordinary differential equation in the radial coordinate. To directly put this in relation with the partial differential equations considered in the present work would require to adopt time independent boundary conditions. In case of slow collective oscillations in the presence of vacuum mixing those would typically be given by a pure flavor state. In case of fast collective oscillations without vacuum terms the boundary conditions would be almost pure flavor states with small off-diagonal terms that are time independent in the standard frame, and rotating with frequency λ in the rotating frame. In the latter case this induces a λ dependence after all, even though λ can still be eliminated from the partial differential equation. This is quite different from the boundary conditions we use here and which in particular allow nontrivial time evolution at the boundaries. The case of stationary solutions can, therefore, not directly be compared with the time dependent scenarios of our present work. This also shows us that the solutions can significantly depend on the chosen boundary conditions.

Coming back to the Liouville-type equation with collision terms Eq. (3), it is less clear if the matter term can also be rotated away in case of a spatially inhomogeneous matter term. Naively one might expect that this

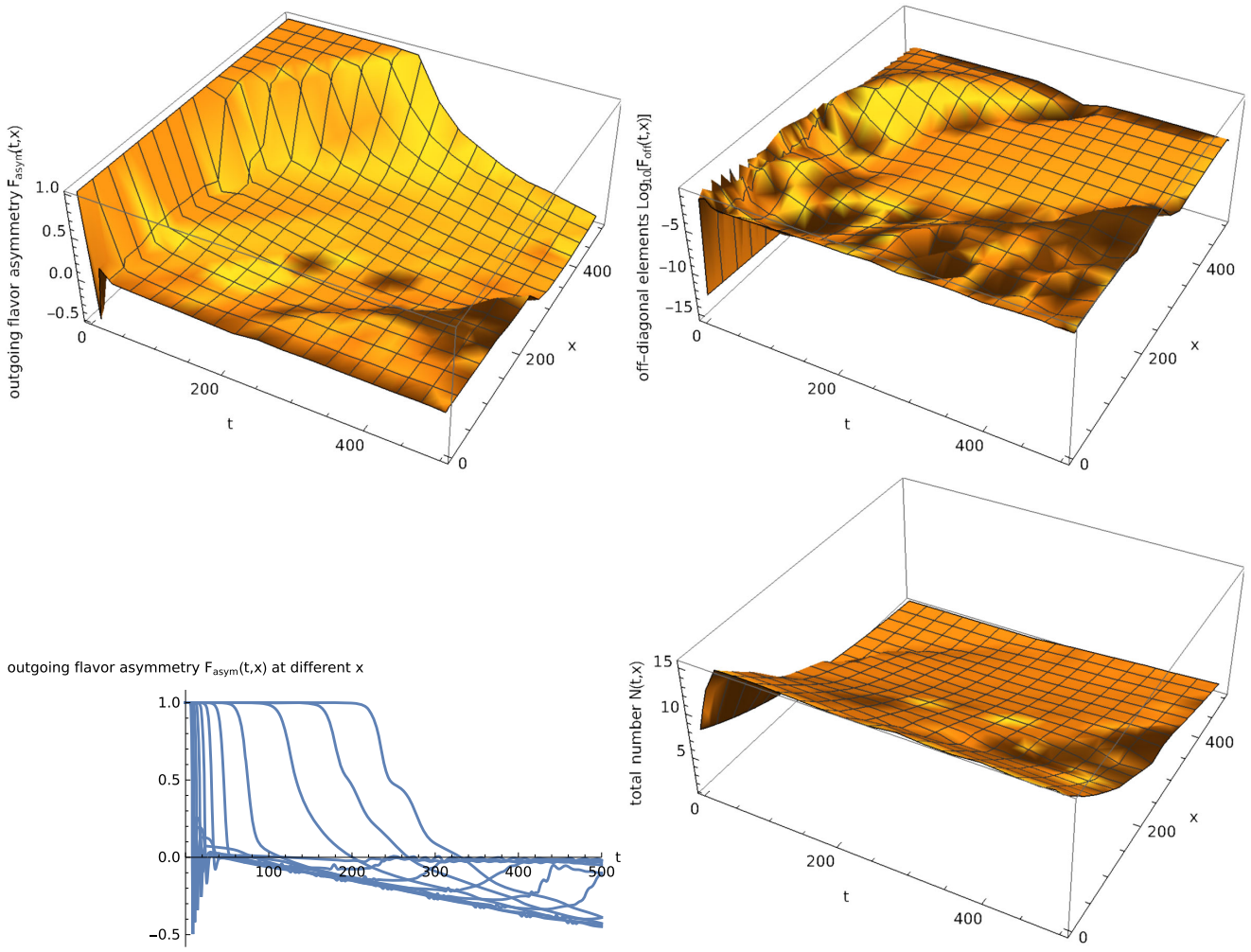

FIG. 10. Results for case (8) simulation which represents a "slow" flavor conversion scenario starting with an inital pure flavor state and inverted hierarchy vacuum terms with $\Delta m^2 = 0.1$, $\theta_0 = 10^{-4}$, and otherwise identical parameters to case (4).

should still be a reasonably good approximation as long as the spatial scale d on which the rates entering the problem vary satisfies $\lambda(\mathbf{r}) \gg 1/d$ in the sense that the variations are then adiabatic. Our simulations show, however, that even in the case $\lambda(\mathbf{r}) \sim 50$, $d \sim 250$, i.e., $\lambda(\mathbf{r}) \sim 10^4/d$ and in the absence of vacuum terms the matter term has a discernible effect and tends to slow down fast flavor conversions. This can be seen by comparing Fig. 2 with Figs. 3 and 5 with Fig. 6. It is thus possible that small scale variations of rates, induced for example by turbulent motion, may have a significant effect on collective flavor oscillations.

We also found significant effects of neutral current scattering on flavor evolution. In Fig. 7 we see that when neutral and charged current interactions occur with comparable rates, significant flavor conversions only take place at small radii where $\mu(x)$ is large. In addition, those conversions do not propagate to the outer boundary, so that the neutrino flux leaving the system is essentially still of pure flavor 1. Isotropic scattering tends to smooth out the crossing of the flavor-lepton number asymmetry which drives fast oscillations, as can be seen in Fig. 9. This is the main reason why scattering tends to suppress fast flavor conversions. Interestingly, we found that if one increases the neutral current scattering rate by a factor 10 (not shown here) the isotropization becomes so efficient close to $x = 0$ that neutrinos stay essentially in the flavor 1 state even around the inner boundary. Furthermore, when both a matter term and nonforward neutral current scattering are present simultaneously, any fast flavor conversions seem to be completely prohibited, as is seen in Fig. 8.

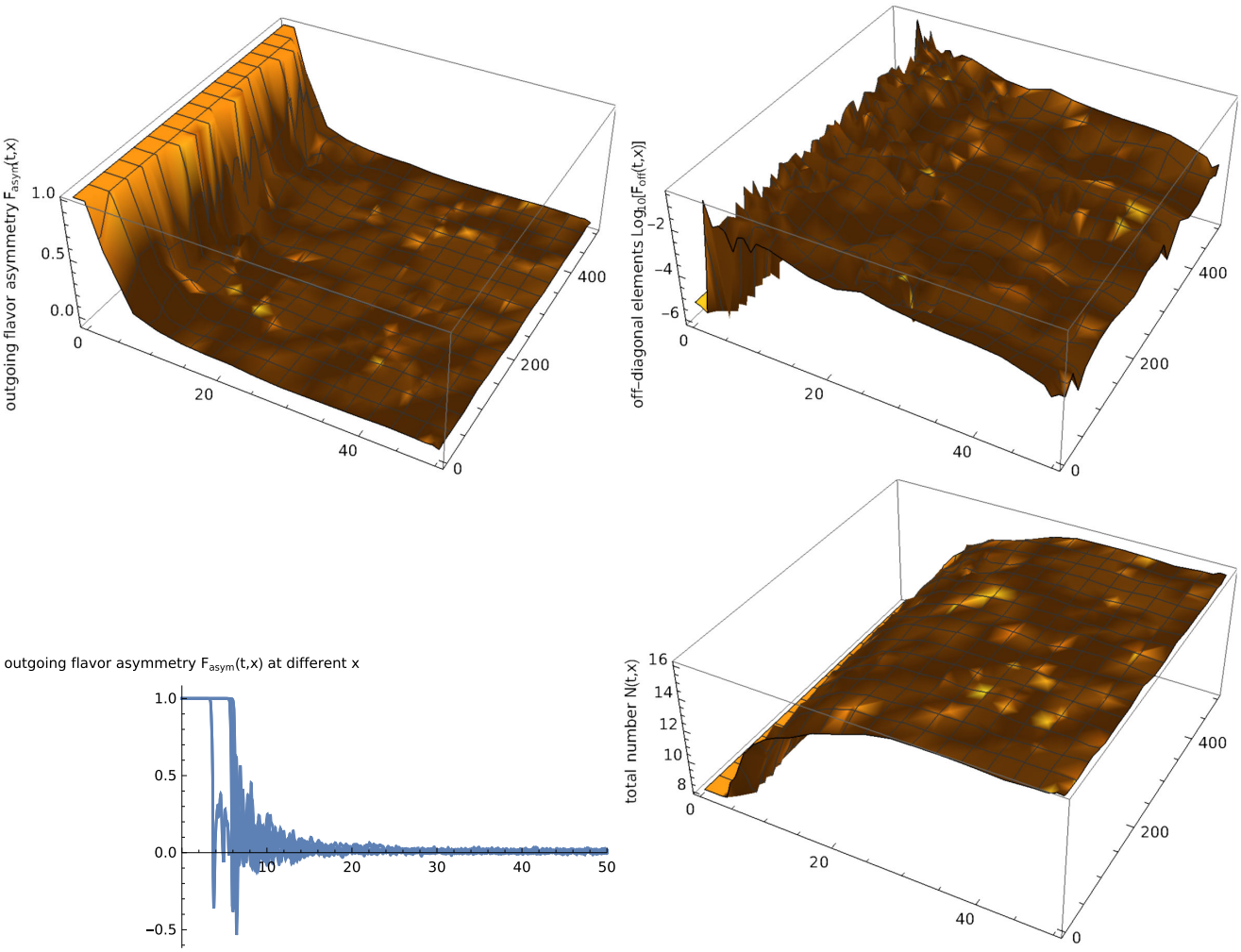

FIG. 11. Results for case (9) simulation for a homogeneous scenario without profile for the rates $\mu(x) = 50$, $\lambda(x) = 0$, $f_{\rm NC}(x) = 0$, and periodic boundary conditions, and otherwise identical parameters to case (4). See the text for details on the initial conditions. Note that the time integration range is much smaller than in the figures for cases (1–8).

Finally, let us discuss the role of neutral current scattering in flavor evolution in the homogeneous case where the problem is reduced to a system of ordinary differential equations as in Refs. [27,35]. Comparison of Figs. 11 and 12 shows no significant influence of neutral scattering for a rate $f_{\rm NC}(x) = 0.1$. Furthermore, similar to the case with profiles, we found a strong suppression of flavor conversions for scattering rates increased by a factor 10 also in the homogeneous case (not shown). In contrast, Refs. [27,35] found situations in which scattering can lead to enhanced flavor conversions in the homogeneous case, typically in the limit of collision rates much smaller than μ, $f_{\rm NC}/\mu \lesssim 10^{-5}$, and sufficiently large vacuum oscillation terms. That we did not find such an enhancement in the homogeneous case shown in Figs. 11 and 12 is because we assumed relatively large collision terms, $f_{\rm NC}/\mu \simeq 0.002$, which tend to erase the electron lepton number crossings before the nonlinear regime is reached, consistent with Ref. [27]. In addition, we do not include a vacuum term. Our findings for the homogeneous case are thus overall consistent with Refs. [27,35].

Our framework also allows to simulate other cases such as density matrices for more than two flavors, inclusion of momentum modes with different energies and a realistic implementation of neutrino pair processes due to neutral current interactions, as well as cases with a global asymmetry between neutrinos and antineutrinos. We leave a more systematic investigation of such cases and a more detailed discussion of so-called slow flavor conversions in the presence of vacuum oscillation terms, in particular in the inhomogeneous settings studied here, to future work.

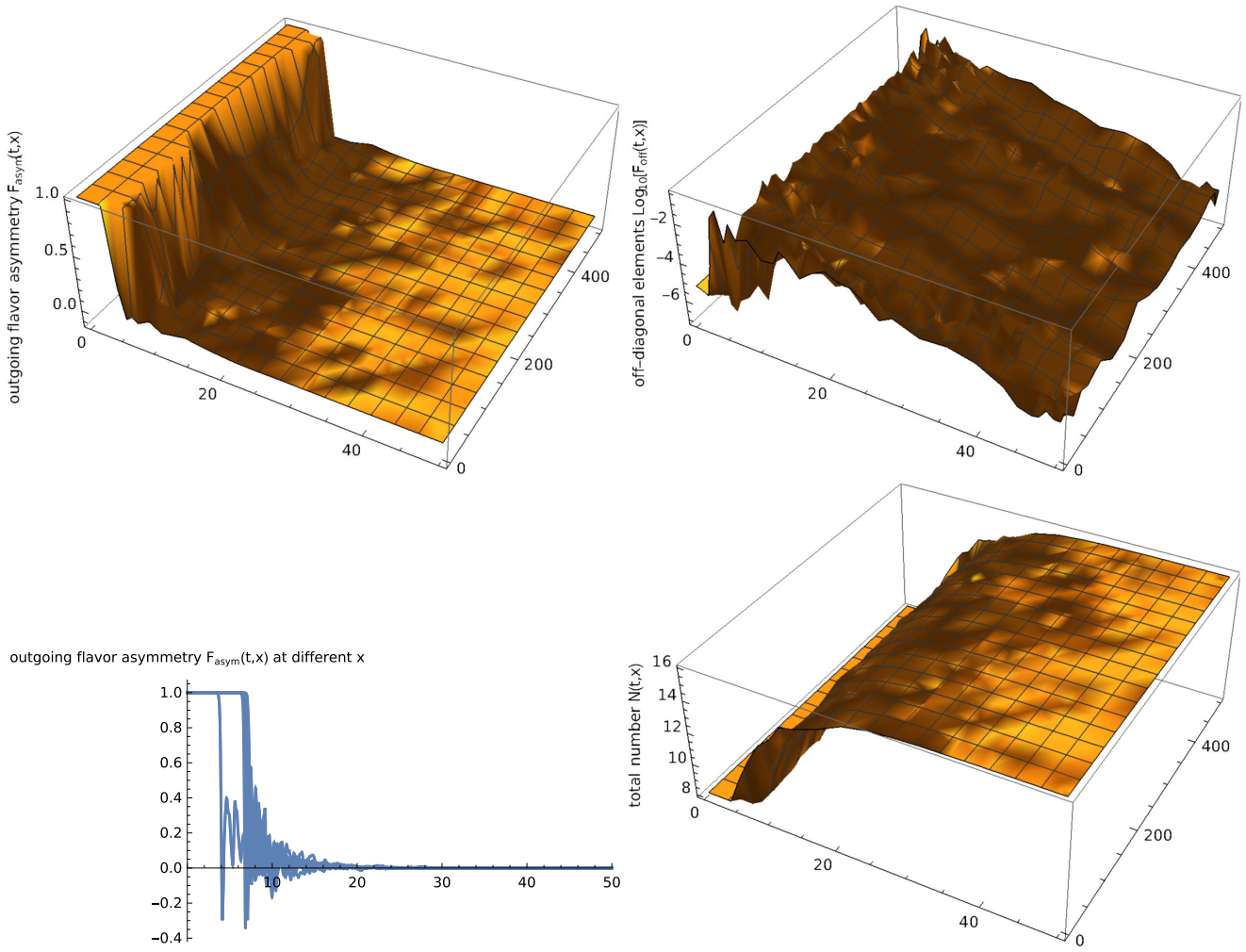

FIG. 12. Results for case (10) simulation for a homogeneous scenario without profile for the rates $\mu(x) = 50$, $\lambda(x) = 0$, $f_{\mathrm{NC}}(x) = 0.1$, and periodic boundary conditions, and otherwise identical parameters to case (4). See the text for details on the initial conditions. Note that the time integration range is much smaller than in the figures for cases (1–8).

VI. CONCLUSIONS

In this paper we have simulated collective neutrino oscillations in the context of inhomogeneous rates for the forward-scattering self-interactions and matter potential, as well as for charged current production and absorption and neutral-current nonforward scattering. Those rates were chosen with a hierarchy that mimics the case of a core collapse supernova close to the neutrino sphere and profiles that fall off with increasing radius. We found a considerable influence of inhomogeneous matter induced refractive terms and neutral current non forward scattering on collective neutrino oscillations with a tendency to suppress or delay in particular fast flavor conversions, in particular if both are present. Furthermore, solutions can depend significantly on the boundary conditions. We do not pretend that the simulations performed here are directly applicable to the situation of a core collapse supernova. However, in our opinion these findings should serve as a warning that such effects should be taken into account in any realistic treatment of collective neutrino oscillations.

ACKNOWLEDGMENTS

G. S. acknowledges support by the Deutsche Forschungsgemeinschaft (DFG, German Research Foundation) under Germany's Excellence Strategy—EXC 2121 "Quantum Universe"—390833306. We also acknowledge numerous insightful discussions on the subject of collective neutrino oscillations with Sajad Abbar, Francesco Capozzi, Basudeb Dasgupta, George Fuller, Alessandro Mirizzi, Georg Raffelt, Shashank Shalgar, Irene Tamborra, and many others.

[1] S. Hannestad, G. G. Raffelt, G. Sigl, and Y. Y. Y. Wong, Self-induced conversion in dense neutrino gases: Pendulum in flavour space, Phys. Rev. D **74**, 105010 (2006); Erratum, Phys. Rev. D **76**, 029901 (2007).
[2] H. Duan, G. M. Fuller, and Y.-Z. Qian, Collective neutrino flavor transformation in supernovae, Phys. Rev. D **74**, 123004 (2006).
[3] G. G. Raffelt and A. Y. Smirnov, Adiabaticity and spectral splits in collective neutrino transformations, Phys. Rev. D **76**, 125008 (2007).
[4] G. G. Raffelt and A. Y. Smirnov, Self-induced spectral splits in supernova neutrino fluxes, Phys. Rev. D **76**, 081301 (2007); Erratum, Phys. Rev. D **77**, 029903 (2008).
[5] H. Duan, G. M. Fuller, J. Carlson, and Y.-Z. Qian, Neutrino Mass Hierarchy and Stepwise Spectral Swapping of Supernova Neutrino Flavors, Phys. Rev. Lett. **99**, 241802 (2007).
[6] G. L. Fogli, E. Lisi, A. Marrone, and A. Mirizzi, Collective neutrino flavor transitions in supernovae and the role of trajectory averaging, J. Cosmol. Astropart. Phys. 12 (2007) 010.
[7] J. D. Martin, J. Carlson, and H. Duan, Spectral swaps in a two-dimensional neutrino ring model, Phys. Rev. D **101**, 023007 (2020).
[8] R. F. Sawyer, Speed-up of neutrino transformations in a supernova environment, Phys. Rev. D **72**, 045003 (2005).
[9] R. F. Sawyer, The multi-angle instability in dense neutrino systems, Phys. Rev. D **79**, 105003 (2009).
[10] I. Izaguirre, G. Raffelt, and I. Tamborra, Fast Pairwise Conversion of Supernova Neutrinos: A Dispersion-Relation Approach, Phys. Rev. Lett. **118**, 021101 (2017).
[11] F. Capozzi, B. Dasgupta, E. Lisi, A. Marrone, and A. Mirizzi, Fast flavor conversions of supernova neutrinos: Classifying instabilities via dispersion relations, Phys. Rev. D **96**, 043016 (2017).
[12] S. Airen, F. Capozzi, S. Chakraborty, B. Dasgupta, G. Raffelt, and T. Stirner, Normal-mode analysis for collective neutrino oscillations, J. Cosmol. Astropart. Phys. 12 (2018) 019.
[13] H. Duan, G. M. Fuller, and Y.-Z. Qian, Collective neutrino oscillations, Annu. Rev. Nucl. Part. Sci. **60**, 569 (2010).
[14] S. Chakraborty, R. Hansen, I. Izaguirre, and G. Raffelt, Collective neutrino flavor conversion: Recent developments, Nucl. Phys. **B908**, 366 (2016).
[15] I. Tamborra and S. Shalgar, New developments in flavor evolution of a dense neutrino gas, Annu. Rev. Nucl. Part. Sci. **71**, 165 (2021).
[16] J. D. Martin, C. Yi, and H. Duan, Dynamic fast flavor oscillation waves in dense neutrino gases, Phys. Lett. B **800**, 135088 (2020).
[17] S. Bhattacharyya and B. Dasgupta, Fast Flavor Depolarization of Supernova Neutrinos, Phys. Rev. Lett. **126**, 061302 (2021).
[18] S. Abbar, H. Duan, K. Sumiyoshi, T. Takiwaki, and M. C. Volpe, Fast neutrino flavor conversion modes in multidimensional core-collapse supernova models: The role of the asymmetric neutrino distributions, Phys. Rev. D **101**, 043016 (2020).
[19] S. Abbar, Turbulence fingerprint on collective oscillations of supernova neutrinos, Phys. Rev. D **103**, 045014 (2021).
[20] G. Mangano, A. Mirizzi, and N. Saviano, Damping the neutrino flavor pendulum by breaking homogeneity, Phys. Rev. D **89**, 073017 (2014).
[21] L. Stodolsky, On the treatment of neutrino oscillations in a thermal environment, Phys. Rev. D **36**, 2273 (1987).
[22] J. F. Cherry, J. Carlson, A. Friedland, G. M. Fuller, and A. Vlasenko, Neutrino Scattering and Flavor Transformation in Supernovae, Phys. Rev. Lett. **108**, 261104 (2012).
[23] S. Sarikas, I. Tamborra, G. Raffelt, L. Hudepohl, and H.-T. Janka, Supernova neutrino halo and the suppression of self-induced flavor conversion, Phys. Rev. D **85**, 113007 (2012).
[24] S. Shalgar, I. Padilla-Gay, and I. Tamborra, Neutrino propagation hinders fast pairwise flavor conversions, J. Cosmol. Astropart. Phys. 06 (2020) 048.
[25] V. Cirigliano, M. W. Paris, and S. Shalgar, Effect of collisions on neutrino flavor inhomogeneity in a dense neutrino gas, Phys. Lett. B **774**, 258 (2017).
[26] F. Capozzi, B. Dasgupta, A. Mirizzi, M. Sen, and G. Sigl, Collisional Triggering of Fast Flavor Conversions of Supernova Neutrinos, Phys. Rev. Lett. **122**, 091101 (2019).
[27] S. Shalgar and I. Tamborra, A change of direction in pairwise neutrino conversion physics: The effect of collisions, Phys. Rev. D **103**, 063002 (2021).
[28] J. D. Martin, J. Carlson, V. Cirigliano, and H. Duan, Fast flavor oscillations in dense neutrino media with collisions, Phys. Rev. D **103**, 063001 (2021).
[29] L. Johns, Collisional flavor instabilities of supernova neutrinos, arXiv:2104.11369.
[30] S. Shalgar and I. Tamborra, Three flavor revolution in fast pairwise neutrino conversion, Phys. Rev. D **104**, 023011 (2021).
[31] T. Stirner, G. Sigl, and G. Raffelt, Liouville term for neutrinos: Flavor structure and wave interpretation, J. Cosmol. Astropart. Phys. 05 (2018) 016.
[32] G. Sigl and G. Raffelt, General kinetic description of relativistic mixed neutrinos, Nucl. Phys. **B406**, 423 (1993).
[33] B. Dasgupta, Collective neutrino flavor instability requires spectral crossing, arXiv:2110.00192.
[34] A. Esteban-Pretel, A. Mirizzi, S. Pastor, R. Tomas, G. G. Raffelt, P. D. Serpico, and G. Sigl, Role of dense matter in collective supernova neutrino transformations, Phys. Rev. D **78**, 085012 (2008).
[35] H. Sasaki and T. Takiwaki, Dynamics of fast neutrino flavor conversions with scattering effects: A detailed analysis, arXiv:2109.14011 [Phys. Rev. D (to be published)].